DETECTION, ANALYSIS AND RISK ASSESSMENT OF COAL FIRES IN NORTHERN CHINA (ID 5345)

Christian Fischer[(1)], Jing Li[(2)], Jianjun Wu[(3)], Christoph Erhler[(1)], Weiguo Jiang [(3)], Shan Guo [(4)], Bo Yang[(5)]

[(1)]German Aerospace Center, German Remote Sensing Data Center, Dept. Land Surface, Germany, email: c.fischer@dlr.de, christoph.ehrler@dlr.de
[(2)] State Key Laboratory of Earth Surface Processes and Resource Ecology, Beijing Normal University, Beijing 100875,P.R. China, email: lijing@bnu.edu.cn
[(3)] Academy of Disaster Reduction & Emergency Management, Beijing Normal University, Beijing 100875, P.R. China, email: jjwu@bnu.edu.cn, jiangweiguo@bnu.edu.cn
[(4)] Chinese Academy of Science, Institute for Remote Sensing Applications, P.O. Box 9718, Beijing P.R. China, email: guoshan@irsa.ac.cn
[(5)] College of Resource and Environment Science, Hunan Normal University, Changsha 410081, P.R. China, email: yangbo@hunnu.edu.cn

ABSTRACT

Uncontrolled combustion of coal is a serious problem on a global scale. Since coal can easily be oxidized and often has a prominent "self-heating" capacity, many coal types have a tendency to combust spontaneously once sufficient oxygen is available and natural cooling is prevented. The rapid expansion of uncontrolled small-scale coal mining activities during the last 30-40 years and the increasing amount of not adequate closed down and now abandoned coal mine sites are supposed to have led to an increase of human-induced coal fires. Thus, coalfield fires need to be not only inventoried at regional scales through rapid and cost effective methods, but also assessed, monitored and secured, wherever appropriate. This leads to major research and technological development objectives: Easy-to-use, routine remote and in-situ monitoring techniques, based on airborne and space borne imagery, to become part in an integrated long-term monitoring framework.

1. INTRODUCTION

Comprehensive studies have focused on two different regions located in the Ningxia Hui Autonomous Region and in the Xinjiang Uyghur Autonomous Region. Both areas under investigation are heavily affected by severe coal fires since years on different places within the coalfields. Besides subsurface coal fires, surface coal fires occur directly on outcropping seams and on places where small-scale mining took place.

The determination of the fire radiative energy (FRE) has been introduced as a remote sensing technique to quantify forest and grassland fires. Various methods for fire detection and FRE quantification have been developed, which can be categorized into single-band algorithms and multi-band algorithms. The nowadays commonly used bi-spectral algorithm for thermal imagery was introduced by [1]. It takes advantage of the non-linear nature of the Planck function to calculate fire temperature and fire size on a sub-pixel basis. This bi-spectral fire temperature and fire area can be used to estimate FRE [2]. In contrast [3] uses a single band algorithm to directly derive FRE of a sub-pixel fire component. In opposite to burning vegetation fires, the coal fire radiative energy (CFRE) is comparably small as most fires are covered by bedrock. Reference [4] conducted a sensitivity study on the ASTER, ETM+ and BIRD TIR satellite sensor systems and found ASTER and ETM+ suitable for energy release quantification using a single band method. Single band methods rely on the robust demarcation of background pixels and fire influenced anomalous pixels. Algorithms for an automatic extraction of local coal fire related anomalies, applicable on LANDSAT, ASTER and MODIS has been developed by [5] and [6], allowing the extraction of thermally anomalous pixels with regard to their surrounding background temperature.

A long-term monitoring and CFRE quantification analysis on multiple temporal separated TIR scenes is feasible only when a reliable fire pixel identification independent from environmental factors can be guaranteed. However, all coal fire anomaly detection algorithms have problems in distinguishing between coal fire induced thermal anomalies and anomalies induced by ambient conditions like inhomogeneous surface heating by the irradiation of the sun. Limited repeatability of the anomaly detection due to atmospheric and climatic influences is a further challenge. Finally a satellite TIR data set is not determined exclusively by the situation at recording time but also by the history of environmental factors which may lead to energy accumulations.

Based on comprehensive field work activities, the following aspects have been considered in detail: (i) different emissivity values of typical rocks covering the

Proc. 'Dragon 2 Final Results & Dragon 3 Kick-Off Symposium' Beijing, P.R. China (ESA SP-704, January 2013)

fire zones, (ii) solar radiation budget that influences the temperature of the topographic surface and corresponding emissions, especially at night time and (iii) the energy balance of the surface itself, as a result of weather conditions and local surface parameters. Simultaneous grid based surface and subsurface.

2. SURFACE ENERGY BALANCE

Usually coal fires burn in the underground resulting in a surface thermal anomaly, which is highly dependent on modifications due to heat conduction and heat capacity of the covering bedrock. Also weather conditions and sunlight exposure show a strong impact. To improve the understanding of this complex atmosphere-surface-subsurface system, an energy balance model for the topographic surface was implemented. The model consists of three linked parts, which are (i) attenuation of solar irradiation in the atmosphere, (ii) energy conversion at the surface and (iii) dissemination of temperature in the subsurface. This approach seems suitable for the mostly arid regions of the Northern Chinese coal belt.

Attenuation of solar irradiation in the atmosphere

A simplified clear-sky atmosphere model is used in part (i). Based on [7] some changes are made primarily to enhance the accuracy and numerical robustness. A set of wavelength independent atmospheric transmission coefficients is calculated from latitude, season and local time of the modelled area encompassing Rayleigh scattering, aerosol scattering and absorption as well as absorption due to water vapour, ozone and atmospheric gases. These coefficients are used in the atmospheric correction algorithm to split top-of-the-atmosphere solar irradiance into attenuated direct and diffuse components. This model is based on standard atmospheric conditions and empirical correlations. It can be easily enhanced if additional data are available, e.g. total water vapour column, cloud coverage and sunshine hours, measured at regular times using MODIS or MERIS data sets, or even better by possible access to more detailed and continuously recorded weather information.

Energy conversion at the surface

Various energy balance terms are modelled in part (ii) including shortwave and longwave balance, sensible heat flux density $E_{sensible}$ and ground heat flux density E_{ground}. The net radiation flux density E_{net} is the sum of all incoming and outgoing radiant flux densities – shortwave and longwave. Effects of elevation, orientation and slope on E_{net} are considered, which include self shadowing, ground reflected irradiation and incident angle. Focus has been set on arid desert-like environments thus the latent heat flux density E_{latent} is not modelled. Sensible heat flux density $E_{sensible}$ is calculated using the bulk aerodynamic method (3) with the constants air density pa (kg m-³) and specific heat of air at constant pressure Ca (J kg-1 K-1). The driving force of the heat exchange is the temperature gradient between surface and air Ts - Ta (K). The aerodynamic resistance ra (s m-1) is dependent on wind speed and surface roughness.

$$E_{sensible} = p_a \cdot C_a \cdot \frac{T_s - T_a}{r_a} \tag{3}$$

In case the wind speed approaches zero the turbulent heat transfer process ceases and aerodynamic resistance ra approaches infinity. This virtually stops any energy loss of the surface due to sensible heat flux.

$$E_{net} + E_{sensible} + E_{latent} + E_{ground} = 0 \tag{4}$$

The total energy balance at the topographic surface for bare soil is given by equation (4). In theory the balance is closed, real measurement attempts however show a gap E_{gap} which encompasses not only errors in measurement but also in methodology (e.g. surface energy storage, scale effects, etc.). In the model this deviation E_{gap} from the energy equilibrium is used to compute a correction offset ΔT for the temperature estimate of the surface layer.

$$E_{gap} \sim \Delta T \tag{5}$$

Formula (6) relates surface layer temperature change ΔT (K) over a time interval dt (s) to the energy equilibrium deviation E_{gap} (W m^{-2}). The heat capacity Cs (J m^{-3} K^{-1}) introduces rock specific warming behaviour into the formula.

$$\frac{dT}{dt} = \frac{E_{gap}}{z * C_s}$$

$$T_t = T_{t-1} + \frac{\Delta t}{z * C_s} \cdot E_{gap} \tag{6}$$

Here the layer thickness z (m) characterizes a hypothetical affected soil volume which gains or loses an energy amount E_{gap} leading to a change in temperature). However difficulties arose in calibrating z to a certain value using field data.

Reference [8] present another calculation approach using fractional integration proposing that the ground heat flux density is completely determined by the history of surface soil temperature. In reverse, when given the soil heat flux density Es, the soil temperature

T_g can be calculated. For the surface it leads to formula (7). Assuming that only the deviation E_{gap} from the energy equilibrium can cause a change in surface temperature and that it acts like an additional flux density in the upper layer then solving the integral for the discrete time step [0…t] gives expression (8).

$$T_g(t) = T_0 + \frac{1}{\sqrt{\pi \cdot k_s C_s}} \int_0^t \frac{E_s}{\sqrt{t-s}}\, ds \tag{7}$$

and

$$T_t = T_{t-1} + \frac{2\sqrt{\Delta t}}{\sqrt{\pi \cdot k_s C_s}} \cdot E_{gap} \tag{8}$$

This formula is in analogy to formula (6) but bypasses the need of introducing a new variable to be determined empirically. Another advantage is the reduced sensitivity to errors in the estimate of the rock specific parameters volumetric heat conductivity ks (J m^{-1} s^{-1} K^{-1}) and heat capacity Cs (J m^{-3} K^{-1}) due to the square root dependence

Dissemination of temperature in the subsurface

Part (iii) utilizes the method of implicit Euler finite differences (9) for modelling the heat conduction in vertical direction through the subsurface layers [9]. Discrete steps in time Δt and space Δz span up a time-space grid. Starting from an initial condition (a given temperature profile at time t=0) and boundary conditions (temperature at surface z=0 and bottom z=N) for each time-space node in the grid a temperature is calculated. The lower boundary condition is set to a constant temperature assuming no diurnal or annual variations at that depth. For simulating the heat source of a subsurface coal fire this lower boundary condition is set to a higher value. The value of the upper boundary condition is adapted every time step and mimics the diurnal temperature wave. Both boundary conditions and rock specific parameters volumetric heat conductivity k_s (J m^{-1} s^{-1} K^{-1}) and heat capacity Cs (J m^{-3} K^{-1}) determine the temperature profile.

$$-C_s \cdot \frac{\partial T}{\partial t} = -k_s \cdot \frac{\partial^2 T}{\partial z^2} \tag{9}$$

$$-C_s \cdot \frac{T_z^t - T_z^{t-1}}{\Delta t} = 2k_s \cdot \frac{\frac{T_{z+1}^t}{\Delta z_{z+1}} - \frac{T_z^t}{\Delta z_{z+1}} - \frac{T_z^t}{\Delta z_z} + \frac{T_{z-1}^t}{\Delta z_z}}{\Delta z_z + \Delta z_{z+1}}$$

Lacking representative field measurements and determination methods heat convection was not implemented yet. Gas flux measurements have shown that the role of convection can only be described in a limited way up to now, but it is to be considered highly varying. Compared to measurements at other fire locations in Rujiqou and Shuixi Gou matrix emission in Wuda (all areas are located in Ningxia Hui Autonomous Region, P.R. China) was order of magnitude lower owing to the fact of the subsurface being solid sandstone. But the field measurements showed a significant part of the energy to be transported by exhaust gases and corresponding heat convection if a system of fissures and cracks does exist. This non-radiative part as well as all lateral energy fluxes cannot be observed by remote sensing.

Modelling results

Based on the clear-sky irradiance, topography, climate factors and a subsurface heat source the model calculates the surface temperature considering all major energy balance terms for an arid environment. Attenuation and lag of the diurnal surface temperature wave on its way into deeper soil/rock layers is modelled by incorporating the ground heat flux and thus a link between surface temperature and subsurface temperature at arbitrary depth is established, cp. Figure 1.

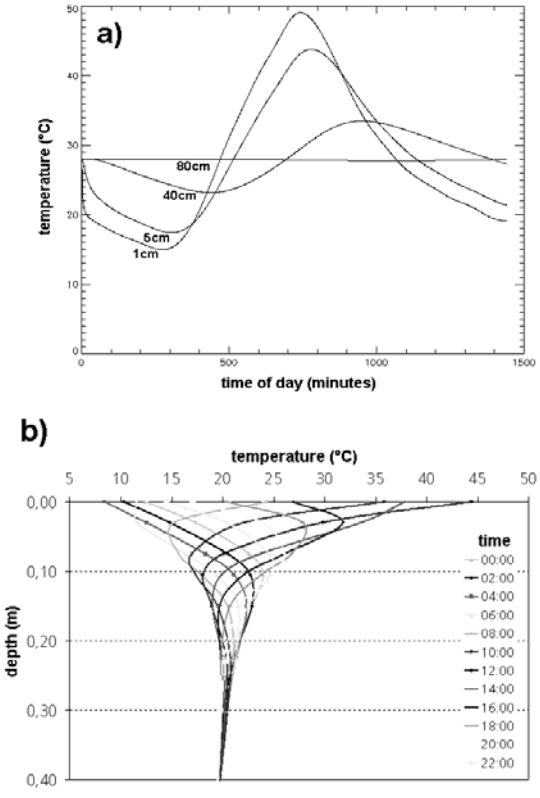

Figure 1: Two examples of modelled soil temperatures for one day. (a) shows the development of soil temperatures at 1cm, 5cm, 20cm and 80cm depth, (b) shows temperature profiles for various times. Damping and phase shift of the diurnal surface temperature wave are clearly visible.

Comparing modelled with measured subsurface temperatures it became obvious that precipitation strongly affects the energy balance by promoting heat conduction and latent heat flux.

3. CFRE SIMULATION

The total emitted energy flux E (W m^{-2}) over all wavelengths of a grey body with emissivity ε (-) and at temperature T (K) can be calculated according to Formula 8, where σ (W m^{-2} K^{-4}) is the Stefan-Boltzmann constant.

$$E = \varepsilon \cdot \sigma \cdot T^4 \tag{8}$$

Using Formula 9 the CFRE can be calculated from the difference in total emitted energy flux E of a grey body at coal fire induced surface temperature T_{fire} and a grey body at background/ambient temperature T_{bg} multiplied by the anomaly area A (m^2).

$$CFRE = \left(E(T_{fire}) - E(T_{bg})\right) \cdot A \tag{9}$$

Feeding the model with the appropriate data a simulation of the surface temperature above a coal fire as well as the site and season specific natural background surface temperature not influenced by the coal fire for any desired time is possible. With the help of Formula (9) a simulated CFRE can be calculated or summed up over a longer period.

4. Potential of various satellite systems for coal fire monitoring

Sensitivity of a specific satellite system to coal fires depends on its spectral bands and resolution as well as on the noise level. At night, which is the most favourable time for coal fire detection, the coal fire radiance can be approximated by the radiance of a black body. Figure 2 illustrates the spectral distribution of the black body radiance as a function of its temperature at typical coal fire surface temperatures from 20 K above the background to 600 K as well as typical spectral bands of satellite sensors in the atmospheric transparency windows in the short-wave infrared (SWIR1: 1.5-1.8 µm and SWIR2: 2.1-2.4 µm), mid-infrared (MIR: 3-5 µm) and thermal infrared (TIR1: 8-9.3 µm and TIR2: 10-13 µm) spectral ranges.

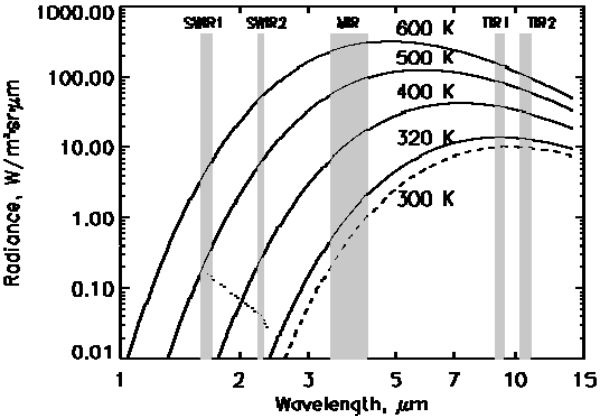

Figure 2: Black body radiance as a function of wavelength and temperature. Shaded are typical spectral bands of satellite imaging systems: SWIR1: 1.6-1.7 µm (ASTER channel 4), SWIR2: 1.235-1.285 µm (ASTER channel 7), MIR: 3.4-4.2 µm (BIRD MIR channel), TIR1: 8.925-9.275 µm (ASTER channel 12), TIR2: 10.25-10.95 µm (ASTER channel 13); the dotted line shows the minimal detectable signal of the ASTER SWIR channels in the high-gain mode; the dashed line represents the radiance of a background with an assumed temperature of 300 K

The sensitivity of various sensors to coal fires are characterized by the fire area $A_{F,min}$ and the coal fire radiative energy that result in the fire/background contrast of e.g. 1.3 (i.e. the signal of the fire pixels is 30% larger than the signal of a background pixel). For the SWIR channels, it is assumed that the fire pixel signal exceeds e.g. by a factor of 3 the minimal detectable signal. These parameters are evidently proportional to the sensor pixel area:

$$A_{F,\min} = q_{\min} \cdot A_{pix}$$

and (10)

$$CFRE_{\min} = \sigma \cdot (T_F^4 - T_{bg}^4) \cdot q_{\min} \cdot A_{pix} = k_{\min} \cdot A_{pix}$$

Where q_{min} is the minimal detectable fire proportion in a pixel, σ is the Stefan-Boltzmann constant, T_F is the fire surface temperature, T_{bg} is the background temperature that is assumed to be equal to 300 K, $k_{\min} = \sigma(T_F^4 - T_{bg}^4) * q_{\min}$ is the minimal detectable SFRP related to the unit pixel area

Here the parameters q_{min} and k_{min} depend only on the sensor bands and on the fire temperature but not on the sensor resolution and thus characterize the sensitivity of various spectral bands regardless of the sensor resolution.

The channels of some satellite sensors, which can be used for coal fire monitoring, are compared in the order of priority in Table 1. The following channels have been analysed:

- SWIR2 (2.235-2.285 µm), TIR1 (8.925-9.275 µm) and TIR2 (10.25-10.95 µm) channels of the Advanced Spaceborne Thermal Emission and Reflection Radiometer (ASTER) on the Terra satellite,
- SWIR2 (2.08-2.35 µm) and TIR2 (10.4-12.5 µm) channels of the Infrared Multispectral Scanner (IRMSS) on the CBERS2 satellite,
- MIR (3.4-4.2 µm) and TIR1 (8.5-9.3 µm) channels of the Bi-spectral Infrared Detection (BIRD) satellite (though the BIRD satellite has stopped functioning, similar cameras will be installed on the TET-1 satellite launched in July 2012),
- SWIR2 (2.105-2.155 µm), MIR (3.93-3.99), TIR1 (8.4-8.7 µm) and TIR2 (10.8-11.3 µm) channels of the Moderate Resolution Imaging Spectroradiometer (MODIS) on the Terra and Aqua satellites.

In spite of the fact that the MIR spectral range is most sensitive to fires, the BIRD MIR channel with a spatial resolution of 370 m is only the third most sensitive channel at all temperatures. At low temperatures close to the background temperature, the most sensitive are the higher-resolution TIR channels of the ASTER and IRMSS sensors, while at a temperature of 400 K or more the most sensitive is the ASTER SWIR2 channel. The IRMSS SWIR2 channel is the second most sensitive channel at a temperature of 500 K or more. The sensitivity of the low-resolution channels of MODIS to coal fires is significantly worse.

Table 1: Minimal detectable fire area and SFRP by satellite sensors [10]]

Fire surface temperature, K	Sensor channel	Resolution, m	Minimal fire area, sq.m	Minimal SFRP, MW
320	ASTER TIR1-TIR2	90	6170 - 7370	0.834 - 0.997
	IRMSS TIR2	160	23800	3,21
	BIRD MIR	370	34900	4,72
	MODIS MIR	1000	268000	36,3
400	ASTER SWIR2	30	298	0,296
	ASTER TIR1-TIR2	90	868 - 1130	0.86 - 1.12
	BIRD MIR	370	1880	1,86
	IRMSS SWIR2	80	3680	3,65
	IRMSS TIR2	160	3740	3,71
	MODIS MIR	1000	15700	15,6
500	ASTER SWIR2	30	12,4	0,038
	IRMSS SWIR2	80	148	0,455
	BIRD MIR	370	269	0,83
	ASTER TIR1-TIR2	90	320 - 448	0.99 - 1.38
	MODIS MIR	1000	2480	7,68
600	ASTER SWIR2	30	1,5	0,01
	IRMSS SWIR2	80	17,2	0,119
	BIRD MIR	370	74,2	0,51
	ASTER TIR1-TIR2	90	173 - 256	1.19 - 1.76
	MODIS MIR	1000	739	5,09

5. CFRE estimation

Based on the investigations described within the previous chapters, a coal fire region next to city of Wuda, Ningxia Hui Autonomous Region, was applied to nine ASTER night time images, which cover all the seasons of year 2007. The multi-temporal ASTER images were co-registered using their geo-referencing information.

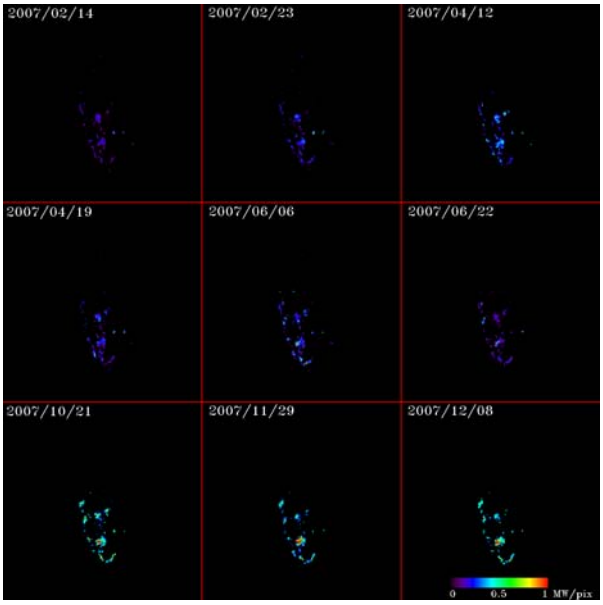

Figure 3:Multi-temporal CFRE analysis of the Wuda coal fire area (calculated CFRE 0-1 MW pixel)

The obtained results show the possibility to detect and monitor coal fires with a high degree of plausibility. The information from the modelled surface energy balance scheme decreases the number of pixels with high uncertainty and pixels showing possible false alarms.

6. RISK ASSESSMENT AT A REGIONAL SCALE

Risk analysis and assessment of underground coal fires at a regional scale play a crucial role in coal fire detection, fighting, and monitoring, and achievements in coal fire mitigation. Results can provide a reasonable scientific guide for fire fighting engineering, and even for resource allocation, ultimately improving the efficiency of fire extinguishing as a whole. They may also be used as input parameters for underground coal fire monitoring and early warning systems.

“Risk” for this and all other purposes describe the possibility of damage or loss. It contains three distinct aspects: (i) the probability of a hazard to occur, (ii) the vulnerability and (iii) the ultimate exposure to the hazard [11] – this is all basic stock of classical risk

theory and has been widely applied in many research fields, especially in those related to disasters [12]. Coal fires, however, are different from other disasters and so "coal fire risk" or "underground coal fire risk" have been newly developed as academic terms for this research field. Their meaning, in fact, may refer to two different types of risk, based on research emphasis: (i) the probability of occurrence of underground coal fires, and (ii) the expected losses of natural resources and environmental as well as human damages brought on by the fires [13] and [14].

Index system

Thus, it has been focused on the first type of risk aiming in quantifying the probability of coal combustion in spatial extent and burning intensity. From the impact factors on regional underground coal fire development, gas content; porosity; coal rank; brittleness; moisture, ash, and sulfur/pyrite content; coal metamorphism; as well as geological age, thickness, and angle of coal seam were selected as evaluation indices for spontaneous combustion tendency. Coal seam depth, faults, anticline, slope/aspect, and fractures were selected as evaluation indices for coal exposure to oxygen. Precipitation and temperature, finally, as well as wind, population density, and mining type and distribution were retained as potential coal fire causes or triggers. Based upon these three index groups, a regional risk assessment index system of underground coal fire development was established.

Methodological Assessment

The method for regional risk assessment of underground coal fire development applied here rests upon three basic operations: data integration and processing, coal fire risk evaluation modelling, and validation. One main pillar of the method is the assessment of spontaneous combustion tendency, coal exposure to oxygen, and analysis of potential fire causes or triggers (see Formulae 11-14). The discrete mechanisms of underground coal fire development, however, are still being researched, and the technologies in use cannot as yet fully identify and distinguish between the contributions of each of these factors. In our study, therefore, we proceeded from the assumption that the impact of each group of indices on coal fire development is of equal value. In order to quantify underground coal fire risk more accurately, spatial overlay was applied to the sum of all indices on a 1km×1km grid, so that risk values for each single grid square could be obtained.:

$$R = V_{combustion} + V_{contact} + V_{cause} \quad (11)$$

$$V_{combustion} = a + a + a + L + a \quad (12)$$

$$V_{contact} = b + b + b + L + b \quad (13)$$

$$V_{cause} = c + c + c + L + c \quad (14)$$

In the formulae above, R is the risk of underground coal fire development at a regional scale. $V_{combustion}$ signifies spontaneous combustion tendency, $V_{contact}$ coal exposure to oxygen, and cause coal fire cause or trigger. $a_1 \sim$ an are n indices of coal spontaneous combustion tendency, $b_1 \sim b_m$ are m indices of coal exposure to oxygen; $c_1 \sim c_k$ are k indices of potential coal fire triggers. The application of the natural break method, a method now extensively used for classification of such data clusters, depended in this case on the distribution of data; results, indeed, maintained their statistical characteristics (ArcGIS 9.0). As applied here, the method worked with five levels of regional underground coal fire risk: no risk, low risk, medium risk, high risk, and extremely high risk. Given that "if there is no coal, there is no coal fire risk"; values for the grid squares outside the coalfield were assumed to be 0. Figure 4 describes the Methodology for risk assessment of underground coal fire development at a regional scale.

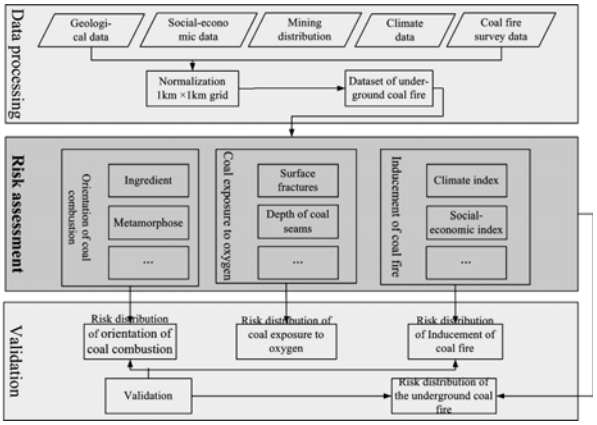

Figure 4: Risk assessment of underground coal fire development at a regional scale

Validation of the method

The spatial distribution of the different underground coal fire risk levels as per under our assessment is shown in Figure 5. No-risk areas are mainly found outside coalfield regions. Extremely high-risk areas are concentrated in northern Xinjiang, from Wusu, Urumchi, and Turfan Basin to Hami; some smaller spots are in the centre, from Baicheng and Luntai to Kuerle and Yangxia, forming a coal fire risk belt.

High risk areas are predominant in Balikun in the eastern parts of Xinjiang, as well as in a line from Wuqia, Yecheng, and Minfeng to Qiemo. In northern Xinjiang, that is, around Tacheng, Kelamayi, and Yili, the risk of underground coal fire development is very low. 20 coal fire zones in Xinjiang have already been extinguished, yet until 2008, another 22 fires were newly discovered [15]. The continued occurrence of coal fires, together with the re-ignition of ancient and (partly) extinguished zones, is a serious challenge to fire fighting activities.

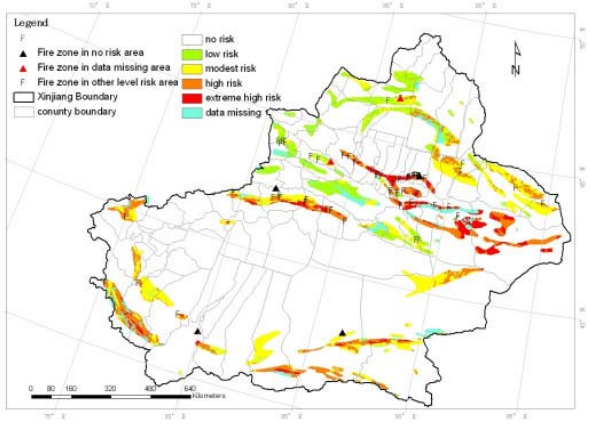

Figure 5: Spatial distribution of underground coal fire risk levels in the province of Xinjiang

For the spatial distribution of underground coal fire risk levels in Xinjiang, the general pattern shows that extremely high coal fire risk are in middle and south part, while low risk distributes in northwest according to the results, fire zone falling into extreme high and high coal fire risk areas can occupy up to 61.54%. There are fewer fire zones falling into low risk coal fire areas. Six fire zones fall into no coal fire risk area, and two of them are falling into the data missing area. The phenomenon is cause of the difference formation time of the fire zone data and coal field boundary data.

7. Conclusions and Recommendations

The presented models bridge the gap so far existing between coal fire modelling in the subsurface using finite element, e.g. as proposed by [16] methods and surface temperature measurements from space. Focusing on remote sensing, the model can assist in validating land surface temperatures derived from remote sensing data and can serve as background for coal fire radiative energy (CFRE) quantifications. With the ability to simulate hot spot temperatures based on in-situ measurements, verification data can be created to critically review CFRE release computed from satellite data. The energy balance model at hand gives a coherent description of the atmosphere-surface-subsurface system. However some aspects are missing, namely latent heat flux and heat transport by convection, limiting the model to arid test sites with compact bedrock. Especially climate data with a high temporal resolution are required to model the variable environmental conditions and their influence adequately. If such data is available in future, implementation of these aspects is straightforward.

The analysis of the multitemporal ASTER TIR data over the Wuda test site shows that multi-temporal processing allows to decrease the TIR threshold for detection of coal seam fires and thus to increase the detectable CFRE. This approach can be used when a sufficiently large observation record covering various seasons is available. Additional tests of the multispectral approach and optimization of its parameters for specific coal fire areas are clearly required and can hopefully be done within upcoming TIR spaceborne missions. One opportunity for further investigations is the BIRD-like experimental small satellite TET-1 carrying an advanced IR system on board. The satellite has been launched by German Aerospace Center in July 2012 and will provide first datasets in 2013.

The Results for regional risk assessment of underground coal fire development in Xinjiang are considered as very satisfying; they may provide very well input for planning and implementing fire fighting campaigns on a macroscopic level in the region.

There are still some details about the method that need further discussion and refinement: first, as regards coal fire causes or triggers, local literacy rate, economic performance and land use type should be included in order to refine human impact analysis and complement the entire index system. Second, though the method is based upon the hypothesis that the contribution of each coal fire risk index is equal, this may not always be the case in reality – for example, human activities may actually have a much larger impact. The weighted value of each index, hence, will be a point of scrutiny in further research.

In order to avoid the further loss of valuable energy resource in the future, long term monitoring, observation and securing techniques needed to be developed, tested and implemented. This include monitoring and control measures for active mining areas associated with a certain risk of spontaneous coal fire ignitions due to the geological deposit structure, natural boundary conditions and human activities, e.g. uncontrolled small scale mining, a monitoring of untouched and unmined coal fields with a notable risk of spontaneous ignitions and an effective and appropriate control of successfully extinguished fire areas/zones to prevent re-ignition dynamics.

ACKNOWLEDGEMENTS

The authors gratefully acknowledge the outstanding support from ESA/MOST during the DRAGON2 programme. DRAGON2 formed an excellent platform for scientific research within an international framework.

The support from Leon Maldonado and the ASTER project science team at Jet Propulsion Laboratory, Pasadena, for providing the ASTER scenes is gratefully acknowledged. The authors also like to thank Mr. Jia Yaorong from Wuhai Energy Co. Ltd and Mr. Cai from the Fire Fighting Bureau in Xinjiang and their teams for the comprehensive support during the field campaigns.

REFERENCES

1. Dozier, J. (1981). A method of satellite identification of surface temperature fields of sub-pixel resolution. *Remote Sensing of Environment*, vol. 11, 221-229.

2. Wooster, M.J., Zhukov, B. & Oertel, D. (2003). Fire radiative energy for quantitative study of biomass burning: derivation from the BIRD experimental satellite and comparison to MODIS fire products. *Remote Sensing of Environment,* vol. 86, 83-107.

3. Kaufman, Y.J., Justice, C.O., Flynn, L.P., Kendall, J.D., Prins, E.M., Giglio, L., Ward, D.E., Menzel, W.P., & Setzer, A.W. (1998). Potential global fire monitoring from EOS-MODIS. *Journal of Geophysical Research*, vol. 103, 32215-32238.

4. Tetzlaff, A. (2004). Coal fire quantification using ASTER, ETM and BIRD satellite instrument data. *Dissertation*, Faculty of Geosciences, Ludwig-Maximilians-University, Munich.

5. Zhukov, B., Lorenz, E., Oertel, D., Wooster, M. & Roberts, G. (2005): Experience of detection and quantitative characterization of fires during the experimental small satellite mission BIRD. *Forschungsbericht 2005-04*, DLR.

6. Künzer, C., Zhang, J., Li, J., Voigt, S., Mehl, H. & Wagner, W. (2007). Detecting unknown coal fires: Synergy of automated coal fire risk area delineation and improved thermal anomaly extraction. *International Journal of Remote Sensing*, vol. 28(20), 4561-4585.

7. Iqbal, M. (1983). *An introduction to solar radiation*. New York, Academic Press.

8. Wang, J., & Bras, R.L. (1999). Ground heat flux estimated from surface soil temperature. *Journal of Hydrology,* vol. 216: 214-226.

9. Rosema, A., Guan, H. & Veld, H. (2000). Simulation of spontaneous combustion, to study the causes of coal fires in the Rujigou Basin. *Fuel,* vol, 80, 7-16.

10. Zhukov, B. (2009). Sensor potential evaluation and algorithm development for detection and radiative power evaluation of coal seam fires. *Internal DLR-Report.*

11. Huang, C.F. (2004). *Risk assessment of natural disaster: Theory & Practice*. Beijing: Science Press.

12. Timothy, W.C., Sara, E.G., Maria de Lourdes & Romo Aguilar. (2009). Vulnerability to environmental hazards in the Ciudad Juarez (Mexico)-EL Paso (USA) metropolis: A model for spatial risk assessment in transnational context. *Applied Geography*, vol, 2, 448-461.

13. Prakash, A. & Vekerdy, Z. (2004). Design and implementation of a dedicated prototype GIS for coal fire investigations in north China. *International Journal of Coal Geology*, vol, 59, 107-119.

14. Peng, G.X., Li J. & Chen, Y.H. (2007). NORIZAN Abdul-patah3 A forest fire risk assessment using ASTER images in peninsular Malaysia. *Journal of China University of Mining & Technology*, vol. 17(2), 232-237.

15. Cai, Z.Y. (2008). Report of investigation of Quergou fire zone in Xinjiang., Xinjiang Coal Fire Fighting and Engineering Bureau. *Internal Report*.

16. Weßling, S. (2007). The investigation of underground coal fires – towards a numerical approach for thermally, hydraulically and chemically coupled processes. *Dissertation*, Department of Electrical Engineering, Information Technology, Physics, Braunschweig University of Technology.